Available online at www.sciencedirect.com
SCIENCE DIRECT®
Journal of Photochemistry and Photobiology A: Chemistry 167 (2004) 149–157
Journal of Photochemistry and Photobiology A:Chemistry
www.elsevier.com/locate/jphotochem

Effects of crystal structure on photolysis of H_2O on K–Ta mixed oxide

Tatsumi Ishihara*, Nam Seok Baik, Naoko Ono, Hiroyasu Nishiguchi, Yusaku Takita

Department of Applied Chemistry, Faculty of Engineering, Oita University, Dannoharu 700, Oita 870-1192, Japan

Received 9 December 2003; received in revised form 19 March 2004; accepted 31 March 2004

Available online 20 July 2004

Abstract

K–Ta mixed oxides with two different crystal structures, i.e. $KTaO_3$ and $K_2Ta_2O_6$, have been prepared by alkoxide and solid-state reaction routes. $K_2Ta_2O_6$ single phase with pyrocrhore like structure can be obtained by the alkoxide method, however, this phase cannot be obtained by a conventional solid-state reaction route. It was found that the prepared $K_2Ta_2O_6$ exhibits the higher activity to photolytic splitting of H_2O into H_2 than that of $KTaO_3$ which is reported as the active catalyst for the H_2O decomposition. Crystalline size of $K_2Ta_2O_6$ pseudo-pyrochlore oxide can be controlled by the hydrolysis condition for alkoxide. It was seen that the crystalline size has a large influence on the photocatalytic decomposition activity and the highest activity was obtained at the crystal size of 30 nm. Effects of metal loading were also investigated on $K_2Ta_2O_6$ oxide and among the examined metals, activity to photolysis of water increased by loading Rh. Formation of oxygen was also observed when 0.2 wt.% Rh was loaded.

Keywords: Photocatalysts; $K_2Ta_2O_6$, $KTaO_3$; Photolysis of water; Crystalline size effects

1. Introduction

Hydrogen is now strongly expecting as a new and clean energy carrier and now produced industrially by the steam reforming reaction of CH_4. However, fairly large energy is required for obtaining hydrogen by steam reforming reaction, because the steam reforming reaction is a large endothermic reaction. Therefore development of hydrogen production process with small energy consumption is an important subject from environmental issues. Photocatalytic decomposition of H_2O into H_2 and O_2 is an ideal reaction for obtaining hydrogen. Therefore, development of an active catalyst for the photocatalytic decomposition of pure water into H_2 and O_2 is strongly required from the viewpoint of energy issues. Various semiconductor oxides, mainly TiO_2 and Nb-based mixed oxides have been investigated extensively as the catalyst for photolysis of water so far [1,2]. Recently, however, various Ta-based oxides are attracting much interest as the new photocatalyst materials, because fairly high activity to the photocatalytic decomposition of H_2O into H_2 and O_2 were reported by Kudo et al. and Sayama et al. [3–5]. In addition, Zou et al. reported that Ni-doped $InTaO_4$ can decompose H_2O into H_2 and O_2 by using visible light [6]. In our previous study, it was found that Zr-doped $KTaO_3$ exhibits the high activity to H_2O photolysis and almost stoichiometric amount of H_2 and O_2 is formed [7,8].

On the other hand, the parameters, which determine the catalytic activity to photolytic splitting of H_2O, have not been still clear. In particular, effects of geometrical properties such as the crystal structure, crystalline and/or particle size, and the surface area on the photocatalytic activity have not been studied systematically excepting for few cases of TiO_2 [9,10], while it is well-known that the geometrical arrangements of atom have a great influence on the catalytic activity in various reactions. Therefore, in the present study, we prepared K–Ta mixed oxides with two different crystal structures, i.e. $KTaO_3$ and $K_2Ta_2O_6$, by the alkoxide method and the conventional solid-state reaction. Effects of crystal structure and the particle size on the photolysis of H_2O were studied systematically. Excepting TiO_2, the effects of crystal structure on the photocatalytic reaction have not been studied, in particular, in case of the mixed oxide consisting of Ta. However, it is noted that TiO_2 with Anatase type exhibits a higher activity to photocatalytic decomposition of H_2O comparing with that of Rutile type [11,12]. Therefore, it is expected that the crystal structure have significant effect on the photocatalytic activity. In this study, the effects of

* Corresponding author. Present Address: Department of Applied Chemistry, Faculty of Engineering, Kyushu University, Hakozaki 6-10-1, Higashiku, Fukuoka 812-8581, Japan. Tel.: +81-92-642-3551; fax: +81-92-651-5606.
E-mail address: ishihara@cstf.kyushu-u.ac.jp (T. Ishihara).

1010-6030/$ – see front matter © 2004 Elsevier B.V. All rights reserved.
doi:10.1016/j.jphotochem.2004.03.030

crystal structure as well as crystalline size on the photolytic splitting of H_2O were studied.

2. Experiment

2.1. Preparation and characterization of K–Ta mixed oxide

Two phases of Ta-based oxides were prepared by two methods, i.e. alkoxide and conventional solid-state reaction. In case of alkoxide method, potassium ethoxide (C_2H_5OK, Wako, 99.99%) and tantalum ethoxide ($Ta(OC_2H_5)_5$, CERAC, 99.999%) were separately dissolved in the ethanol solution under argon atmosphere in a glove box (Dew point <223 K). After mixing these two solutions by a magnetic stirrer sufficiently, the mixture was taken out into air. For the purpose of hydrolysis, small amount of deionized water was slowly dropped to this solution followed by stirring vigorously. The resulting suspension was aged for overnight after stirring for 2 h, and then dried at 348 K. In order to control the crystallite size, the amount of water and temperature for hydrolysis of alkoxide was changed. The obtained powder was then calcined at various temperatures for 6 h in air. In case of the conventional solid-state reaction, aqueous solution of KNO_3 was evaporated with the powder of Ta_2O_5 (Kishida, 99.9%). The obtained powder was mixed again in Al_2O_3 mortar with Al_2O_3 pestle and then calcined at various temperatures in air. Metal loading was performed by using the conventional incipient wetness techniques using aqueous solutions of $Ni(NO_3)_2{\cdot}6H_2O$, $[Pt(NH_3)_4](NO_3)_2$, $[Rh(NH_3)_6]Cl_3$, $Pd(NH_3)_4Cl_2{\cdot}H_2O$, $Ru(C_5H_7O_2)_3$. The obtained metal-loaded catalyst was calcined in air at 623 K for 6 h and reduced in H_2 flow at 748 K for 2 h and then calcined in the oxygen flow at 473 K for 1 h. The crystal structure of the obtained sample was analyzed by X-ray diffraction measurement (XRD, Rigaku Rint 2500) with Cu Kα line. The crystalline size of the sample was estimated by the line broadening method using Scherrer's equation. BET surface areas and the particle size distributions of the sample were analyzed with the conventional gas adsorption method (SP-18S, Nippon Bell Co. Ltd.) and the laser scattering particle size distribution analyzer (LA-920, HORIBA Co. Ltd.), respectively. The shape of the particle was observed by using Field Emissions (FE) SEM (JEOL, JEM-6700F). Photo-absorption property of the sample was measured with the ultraviolet-visible (UV-Vis) diffuse reflectance spectrometer (U-3410, HITACHI). Rietveld analysis of $K_2Ta_2O_6$ was carried out by using the Rietan 94 [13]. Electronic band structure in $K_2Ta_2O_6$ and $KTaO_3$ were calculated by using code "CASTEP (Cambridge Serial Total Energy Package, Accelrys Co. Ltd.)" based on the crystal structure which is estimated by the Rietveld analysis followed by optimizing the crystal structure by energy minimum method. It has been reported that CASTEP gives the band structure in quantitative agreement with other electronic structure calculations [14,15].

2.2. Photocatalytic decomposition reaction of water

Photocatalytic decomposition reactions were carried out in a conventional gas closed circulating system and Ar (ca.13.3 kPa) was used as a carrier gas. The catalyst powder (100 mg) was dispersed in 30 ml of deionized water using a magnetic stirrer in a quartz reaction cell. After adjusting pH of the catalyst suspending solution to 11 by KOH, the reaction cell was irradiated by an external light source of a 500 W Xenon lamp (Ushio). The amount of H_2 and O_2 formed was analyzed by using TCD gas chromatograph connecting to a circulating system. The formation rate of H_2 and O_2 was estimated by using the amount in an initial 6 h.

3. Results and discussion

3.1. Preparation and crystal structure

Fig. 1(b) shows X-ray diffraction patterns of precipitation powders obtained by the alkoxide route after drying or calcination at marked temperature. It is clear that the as-precipitated sample was an amorphous state and no diffraction peak was observed. However, after calcination at 773 K in air, formation of the single crystal phase of $K_2Ta_2O_6$ was observed. With increasing the calcination temperature, diffraction peaks from $K_2Ta_2O_6$ phase became intense and narrowed. Therefore, it is considered that the crystal grows occurred as temperature increases. However, by calcination at 873 K, formation of $KTaO_3$ is observed and the sample was completely transferred to $KTaO_3$ phase after 1273 K calcinations [16]. On the other hand, similar XRD patterns of the powders obtained by the conventional solid-state reaction are shown in Fig. 1(a). It was seen that

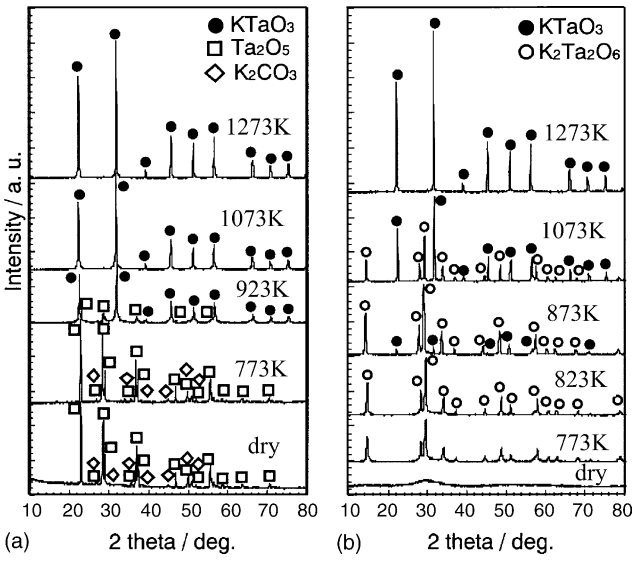

Fig. 1. X-ray diffraction patterns of the K–Ta mixed oxide obtained by hydrolysis of alkoxide (a) and the conventional solid-state reaction; (b) after calcining at the marked temperature.

Table 1
Refined atomic coordinates of $K_2Ta_2O_6$ obtained by the Rietveld analysis.(Space group: Fd3m)

Atom	Occupancy	Atomic coordinates		
		X	*Y*	*Z*
K	1.000	0.65921	0.65951	0.59554
	S.D.	0.0304	0.05014	0.06147
Ta	1.000	0.12229	0.13650	0.12152
	S.D.	0.01108	0.01956	0.05420
O(1)	1.000	0.45384	0.04479	0.75672
	S.D.	0.08376	0.13712	0.10919
O(2)	1.000	0.19041	0.03470	0.19856
	S.D.	0.02278	0.01807	0.02358

S.D. means standard deviation, *R* factor; 13.3%.

the powders obtained by precipitation of KNO_3 to Ta_2O_5 are just mixture of K_2CO_3 and Ta_2O_5 after dry at 343 K. Since K_2O easily reacts with CO_2, it is considered that formation of K_2CO_3 is result of the reaction between K_2O and CO_2 in the atmosphere. Perovskite phase of $KTaO_3$ appeared after calcination at 923 K and the single phase of $KTaO_3$ was obtained by calcination at 1073 K. However, formation of $K_2Ta_2O_6$ cannot be observed by the conventional solid-state reaction. This difference my result from difference in mixing level of K and Ta in precursor. Since the detail analysis of crystal structure of $K_2Ta_2O_6$ is not reported up to now, crystal structure of $K_2Ta_2O_6$ was analyzed in detail by using Reitvelt analysis.

Reitvelt analysis was performed for $K_2Ta_2O_6$ with Fd3 m lattice group. Although it is reported that $K_2Ta_2O_6$ is assigned to Cpp group [17], fitting by this space group is not well agreed in this study. In comparison, diffraction patterns based on Fd3m (No. 227) gives the best fit among the all space groups in this study. It is also noted that the space group for the similar compound of $Na_2Ta_2O_6$ is also reported as Fd3m, which is the same with that used in this study [18]. The final refinement results for atomic coordination of $K_2Ta_2O_6$ are listed in Table 1. Considering the value of *R* factor, 13.3%, it is considered that the atomic coordination of $K_2Ta_2O_6$ is reasonably refined. In Table 2 is also shown a comparison of refined and reported lattice parameter for $K_2Ta_2O_6$ and $KTaO_3$ [17]. The structural analysis results indicated that $K_2Ta_2O_6$ as well as $Na_2Ta_2O_6$ has a pyrochlore-like cubic crystal structures, of which typical compound is $Ca_2Ta_2O_7$.

The refined crystal structure of $K_2Ta_2O_6$ is shown in Fig. 2 in which perovskite structure of $KTaO_3$ is also shown for the comparison. As shown in Fig. 2, crystal structure of $KTaO_3$ is the ideal cubic perovskite structure, of which lattice parameter is 0.39877 nm, since tolerance factor was 0.96. On the contrary, $K_2Ta_2O_6$ is pyrochore like cubic structure consisting of distorted TaO_6 octahedral. The refined lattice parameter is 1.06058 nm which is slightly smaller than that of reported one [19], but in this structure, one oxygen is regularly missing from the ideal pyrochlore structure of $A_2B_2O_7$ considering the composition. Therefore, it is considered that the center for the positive charge might be deviated from that for negative charge in the crystal structure. Furthermore, TaO_6 octahedral is greatly distorted. Although $KTaO_3$ and $K_2Ta_2O_6$ have the same chemical composition, this difference in crystal structure may cause the difference in the electronic band structure resulting in the different photocatalytic activity. It is also noted that the calculated free volume of the unit cell is 16.81×10^{-3} and 28.00×10^{-3} nm^3 for $KTaO_3$ and $K_2Ta_2O_6$, respectively. Packing of the atom in $K_2Ta_2O_6$ is looser than that in $KTaO_3$ and has much larger free volume.

3.2. Electronic band structure configuration of $KTaO_3$ and $K_2Ta_2O_6$

Diffuse reflection spectra of $KTaO_3$ and $K_2Ta_2O_6$ are shown in Fig. 3. Although both oxides have the same composition, it is seen that the onset of $KTaO_3$ greatly differs from that of $K_2Ta_2O_6$. As shown in Fig. 3, $KTaO_3$ and $K_2Ta_2O_6$ have an absorption edge in a ultraviolet region suggesting a wide band gap. Clearly, absorption edge of $K_2Ta_2O_6$ exists at lower wavelength (around 240 nm) than that of $KTaO_3$ (330 nm). Therefore, it is obvious that $K_2Ta_2O_6$ has a wider band gap than that of $KTaO_3$. It is noted that the band gap estimated from UV-Vis absorption edge is 5.2 and 3.9 eV for $K_2Ta_2O_6$ and $KTaO_3$, respectively. It is well known that the electronic configuration in metal oxide strongly depends on the consisting element and its geometric arrangements. Considering the same chemical composition of $KTaO_3$ and $K_2Ta_2O_6$, difference in electronic configuration between $KTaO_3$ and $K_2Ta_2O_6$ could be assigned to the geometrical effects of cation and anion arrangements in the crystal lattice.

Since the great difference in electronic band structure is suggested by photoabsorption spectra, total electronic density of states (DOS) for $K_2Ta_2O_6$ and $KTaO_3$ are calculated based on the crystal structure (Fig. 4). It is seen that a great difference in total DOS is also observed for $KTaO_3$ and $K_2Ta_2O_6$ as suggest by UV-Vis absorption measurement. In

Table 2
Lattice parameter of $K_2Ta_2O_6$ and $KTaO_3$ refined in this study.

	a (nm)	*b* (nm)	*c* (nm)	*α* (°)	*β* (°)	*χ* (°)	Space group
$K_2Ta_2O_6$ (JCPDS card)	1.05961	1.05961	1.05961	90.00	90.00	90.00	Cpp
$K_2Ta_2O_6$ (this study)	1.060582	1.06058	1.06058	90.00	90.00	90.00	Fd3m
$KTaO_3$ (this study)	0.39877	0.39877	0.39877	90.00	90.00	90.00	Pm3m
$Na_2Ta_2O_6$ (ICSD card)	0.39877	1.0442	1.0442	90.00	90.00	90.00	Fd3m

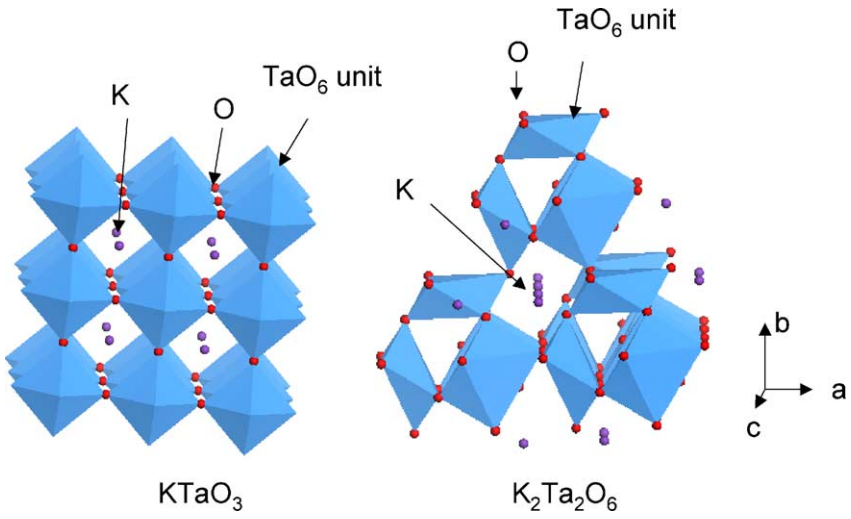

Fig. 2. Crystal structure of $KTaO_3$ and $K_2Ta_2O_6$.

good agreement with the results of UV-Vis absorption data, total DOS calculation based on the functional density quantum calculation suggests that the band gap of $K_2Ta_2O_6$ is twice larger than that of $KTaO_3$. The estimated band gap for $K_2Ta_2O_5$ and $KTaO_3$ is 4.5 and 3.4 eV, respectively. Since the valence and conduction band is O2P and Ta5d respectively for both $KTaO_3$ and $K_2Ta_2O_6$ and the molecular orbital generated from K atomic orbital exists at deep energy level, difference in the band gap could be explained by the different overlapping way of the atomic orbital of tantalum and oxygen. Since $K_2Ta_2O_6$ has a longer Ta–O distance (0.19940 nm) than that in $KTaO_3$ (0.30330 nm), energy level of conduction band becomes higher on $K_2Ta_2O_6$, since overlapping of atomic band is required long distance. Since the relationship between electronic band structure and photocatalytic activity have not been studied in details, the photolysis activity to H_2O decomposition on $K_2Ta_2O_6$ and $KTaO_3$ was compared.

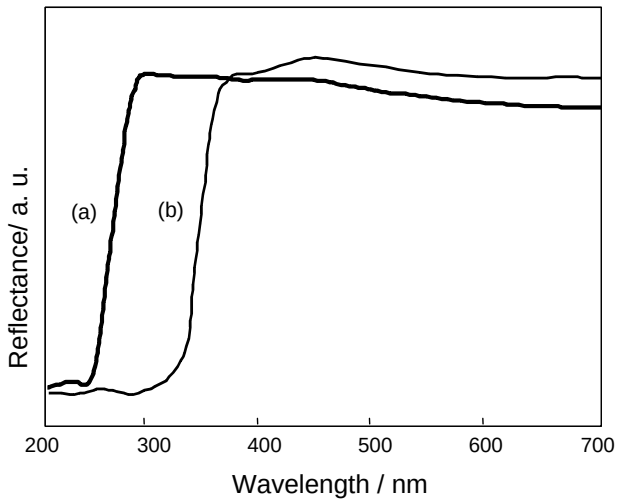

Fig. 3. UV-Vis reflectance spectra of $K_2Ta_2O_6$ (a) and $KTaO_3$(b).

3.3. Photolysis activity of $K_2Ta_2O_6$ and $KTaO_3$ to H_2O splitting

Fig. 5 shows the formation rate of H_2 in photolysis of H_2O as a function of reaction period on $K_2Ta_2O_6$ and $KTaO_3$ prepared by the alkoxide and the conventional solid-state reaction. Formation of oxygen was hardly observed on all catalysts examined, which is in good agreement with our previous results [7,8]. Therefore, activity to photolytic splitting of water was discussed based on the H_2 formation rate in this study. Since no H_2 formation was observed without light irradiation and no carbon impurity was de-

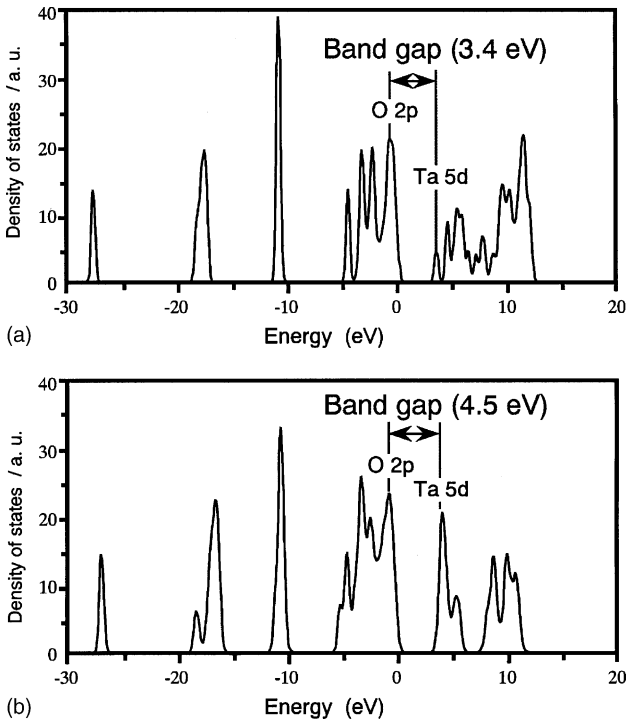

Fig. 4. Electronic density of state (DOS) of $KTaO_3$ (a) and $K_2Ta_2O_6$ (b).

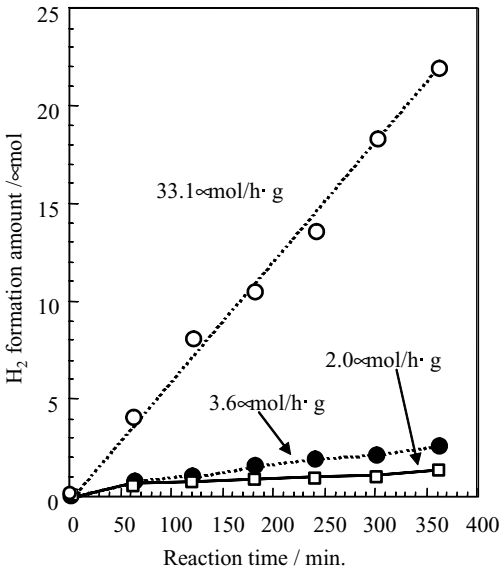

Fig. 5. Photocatalytic decomposition of H_2O on $K_2Ta_2O_6$ and $KTaO_3$, (○) $K_2Ta_2O_6$ prepared by alkoxide method, (●) $KTaO_3$ prepared by alkoxide method, (□) $KTaO_3$ prepared by conventional method.

tected in both $KTaO_3$ and $K_2Ta_2O_6$ samples by X-ray fluorescence (XRF) measurement, it is considered that hydrogen is formed by the photolytic splitting of water. As shown in Fig. 5, it is seen that the H_2 formation rate increased in the following order, $KTaO_3$ (solid-state reaction) < $KTaO_3$(alkoxide) ≪ $K_2Ta_2O_6$. H_2 formation rate of $KTaO_3$ prepared by alkoxide method (3.6 μmol/g h) was much higher than that of $KTaO_3$ prepared by the solid-state reaction method (2.0 μmol/g h), since $KTaO_3$ prepared by alkoxide method has higher crystallinity and larger surface area (5 m^2/g) which was twice larger than that of $KTaO_3$ prepared by the solid-state reaction method (2.5 m^2/g). On the other hand, it was found that $K_2Ta_2O_6$ exhibits higher H_2 formation rate (33.1 μmol/g h) for H_2O decomposition by an order of magnitude comparing with that of $KTaO_3$. Higher formation rate of H_2 on $K_2Ta_2O_6$ could be explained by the larger surface area (about 22 m^2/g), smaller crystalline size (approximately 30 nm) and the different crystal structure. Although the absorption edge of $K_2Ta_2O_6$ exists at the lower wavelength than that of $KTaO_3$, it is interesting that the larger activity to the photolysis of H_2O is achieved on $K_2Ta_2O_6$. This is because the strength of light in UV region is weak in case of Xe light used. Similar phenomena are also reported on $Sr_2M_2O_7$ (M = Ta and Nb) [20]. Comparing the difference in the surface area, the difference in H_2 formation rate between $KTaO_3$ and $K_2Ta_2O_6$ is more significant. Therefore, it seems like that one reason for the larger photolysis activity of H_2O splitting on $K_2Ta_2O_6$ could be assigned to the larger surface area. However, since the octahedral of TaO_6 unit in $K_2Ta_2O_6$ is much distorted (Fig. 2), it is considered that the charge separation could be easier on $K_2Ta_2O_6$ than $KTaO_3$ due to the local polarization effects. These effects by crystal structures are also suggested by Inoue et al. on $BaTi_4O_9$ [21,22] and Kudo et al. on $Sr_2Ta_2O_7$ [20]. In any case, it is seen that $K_2Ta_2O_6$ exhibits much higher activity for photolytic H_2O splitting.

Effects of surface area and/or particle size were further studied on $K_2Ta_2O_6$ catalyst in detail in order to show the crystal structure effects on photolysis of water. $K_2Ta_2O_6$ with different crystallite sizes can be obtained by changing the amount of water for hydrolysis of mixed alkoxide. Fig. 6 shows the XRD patterns of the specimens after calcination at 773 K, which was prepared at the different ratio of H_2O to alkoxide for hydrolysis. It was seen that all diffraction peaks of the sample can be assigned to those from $K_2Ta_2O_6$ and no diffraction peaks from impurity phase were observed. Therefore, single phase of $K_2Ta_2O_6$ was obtained on all samples prepared at different H_2O/alkoxide ratio. Obviously, width of the diffraction peaks becomes narrower and sharper with increasing H_2O amount for the hydrolysis reaction. This result suggests that the crystalline size of $K_2Ta_2O_6$ increases with increasing the amount of water for hydrolysis of alkoxide. Crystallite size was estimated by the line broadening method with Scherrer's equation and shown in Fig. 7 against the ratio of H_2O to mixed alkoxide. It is seen that the estimated crystallite size monotonically increased with increasing the ratio of H_2O to alkoxide. It is also noted that the further larger crystallite sized $K_2Ta_2O_6$ of 50 nm can be obtained by increasing temperature for aging up to 333 K. BET surface area of the specimens is also shown in Fig. 7 as a function of the ratio of added H_2O to alkoxide amount. In good agreement with the tendency of crystallite size on H_2O amount, BET surface area also decreased with increasing the amount of H_2O.

Fig. 8 shows the SEM observation results of the $K_2Ta_2O_6$ particle at the H_2O/alkoxide ratio of 1 and 5. Although the distribution in particle size of $K_2Ta_2O_6$ was observed, it is seen that the particle size of $K_2Ta_2O_6$ at H_2O/alkoxide ratio of 5 is much larger than that at H_2O/alkoxide = 1. Therefore, SEM observation results are in good agreement with those of XRD measurement. In addition, the shape of the particle was slightly different, namely, $K_2Ta_2O_6$ obtained at H_2O/alkoxide = 5 consists of an angulated particle but that at 1 is more sphere shape and uniform size.

The particle size distribution was further studied by the laser distribution method. Fig. 9 shows the comparison of the particle size distribution at the ratio of water to alkoxide of 1, 5, and 10. It is considered that the estimated particle size distribution by the laser distribution method is not primary particle but the aggregated particle size in water, namely, dispersivity. $K_2Ta_2O_6$ in water has two distributions in size, namely, particle distributing around 1 and 6 μm. With increasing the particle size, distribution around 6μm became dominant and particle size distribution was shifted to the larger particles. In particular, average aggregated $K_2Ta_2O_6$ particle obtained at H_2O/alkoxide ratio of 10 is as large as 12 μm. Therefore, it is seen that the high dispersion of particle is achieved with decreasing the particle size.

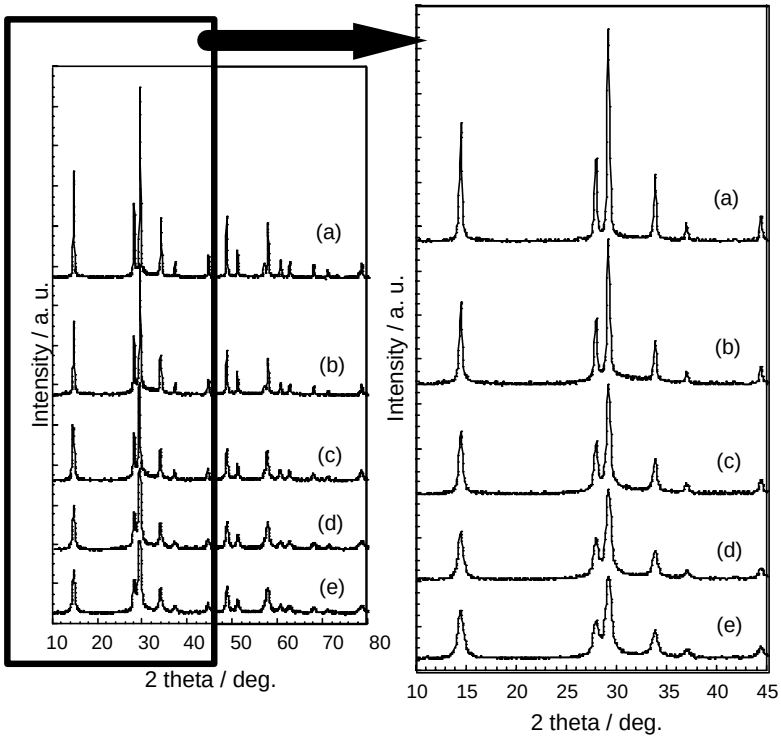

Fig. 6. XRD patterns of the sample at the different H_2O/alkoxide ratio after calcinations at 773 K: (a) 10.0; (b) 5.0; (c) 2.0; (d) 1.0; (e) 0.5.

Fig. 10 shows the effects of crystallite size on H_2 formation rates on $K_2Ta_2O_6$ catalyst. Kudo et al. reported that the surface area is not an important factor in case of tantalates for the H_2O photocatalytic decomposition [23]. However, it is clear that the formation rate of H_2 increased linearly with increasing the crystalline size and it attained a maximum value around 30 nm. Therefore, crystalline size and/or BET surface area show a great influence on the photocatalytic activity of $K_2Ta_2O_6$ to H_2O photolytic splitting. It is generally expected that the catalyst with smaller crystallite is more active because of larger surface area. However, as shown in Fig. 10, dependence of the formation rate of H_2 on the catalyst particle size is opposite to the expectation. It is considered that the amount of the defects at bulk and surface increase as the crystallite size decreases. Since it is generally believed that point defects in lattice tend to trap free electron or hole, probability for trapping the photo-excited electron and/or hole may increase as the particle size decreases. As a result, excessively small crystalline size is not desired from the photocatalytic activity. In contrast, excessively larger crystalline size is also not desired for the photocatalyst, since the diffusion length of the excited electron and hole to the active site becomes longer and the quantum efficiency will decrease at larger particle size due to increase in the probability of recombination of hole and electron. Consequently, the optimized crystal size should exist and this is ca. 30 nm for $K_2Ta_2O_6$. It is also noted that the high dispersion of particle is achieved at this $K_2Ta_2O_6$ with ca.30 nm size (Fig. 11).

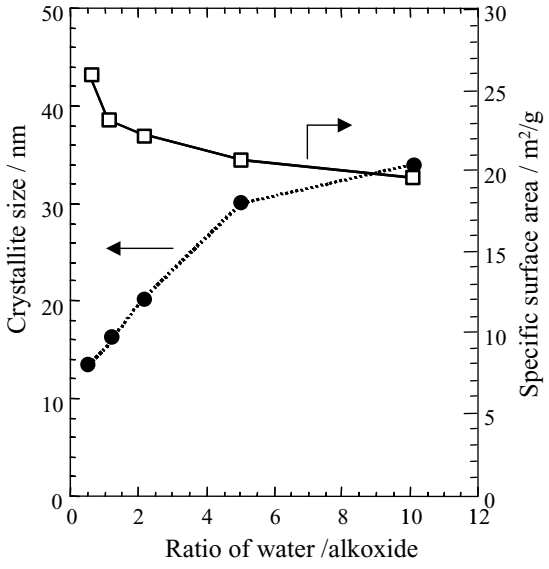

Fig. 7. The estimated crystallite size against the ratio of H_2O to alkoxide.

Effects of metal or metal oxide loading to $K_2Ta_2O_6$ catalyst were further studied. It is reported that loading small amount of metal, in particular, Pt or NiO, greatly improves the photocatalytic activity of oxide [1–5]. In this study, effects of various noble metals or metal oxides were studied on $K_2Ta_2O_6$ and the H_2 formation rate is compared in Fig. 11. It was seen that loading of noble metal or metal oxide unusually decreased the photocatalytic activity of $K_2Ta_2O_6$ to H_2O decomposition. In particular, the H_2 for-

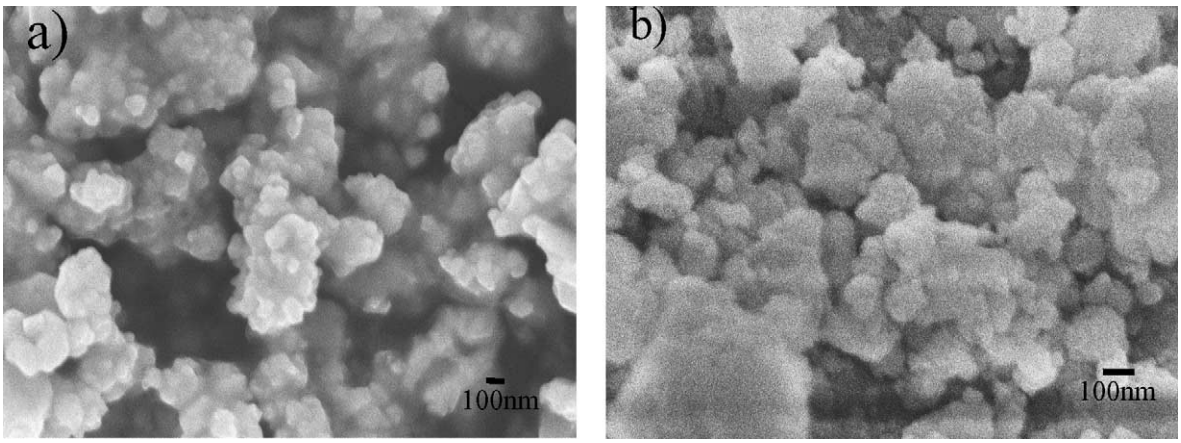

Fig. 8. SEM observation of the $K_2Ta_2O_6$ particle obtained at H_2O/alkoxide = 1 (a) and 5 (b).

mation rate greatly decreased by loading NiO, which is generally the most effective promoter for many photocatalysts [20–24]. The reason for the negative effects of metal loading are not clear up to now. However, considering the wide band gap in K_2TaO_3, the amount of photon usable for photolysis of H_2O may decrease by loading metal. It is also considered that the formed H_2 is oxidized by formed O_2 on the loaded metal. On the other hand, loading small amount of Rh_2O_3 slightly increased the H_2 formation rate. Therefore, it can be said that Rh_2O_3 is the most effective promoter among the metal or metal oxide examined. Effects of the amount of Rh_2O_3 on the photolysis of H_2O on $K_2Ta_2O_6$ were further studied in detail.

H_2 formation rate is shown in Fig. 12 as a function of the amount of Rh_2O_3 loading on $K_2Ta_2O_6$ with the average particle size of 30 nm. It was demonstrated clearly that H_2 formation rate increased with increasing the amount of Rh_2O_3 and attained a maximum value at 0.25 wt.%. Therefore, the optimized amount of Rh loading seems to exist at 0.25 wt.%. Considering that the color of the catalyst becomes black with increasing the amount of Rh_2O_3, excess amount of Rh_2O_3 loading may decrease the amount of UV light coming into $K_2Ta_2O_6$ oxide resulting in the decreased activity to H_2 formation rate.

Fig. 13 shows the amounts of H_2 and O_2 formation as a function of reaction time on Rh_2O_3-loaded $K_2Ta_2O_6$ with 30 nm particle size. As discussed, formation of H_2 was only observed on $K_2Ta_2O_6$ and no O_2 formation was observed. However, it was seen that the formation of O_2 was also observed by loading Rh_2O_3. Therefore, loading Rh_2O_3 is effective for enhancing the photocatalytic activity of $K_2Ta_2O_6$ to H_2O splitting into H_2 and O_2. However, the amount of O_2 is much smaller than that of H_2. As a results, complete decomposition of H_2O cannot be achieved on $Rh_2O_3/K_2Ta_2O_6$ catalyst. At present, the detail mechanism for oxygen consumption are not clear, however, it seems likely that the formed oxygen remind on the catalyst to form the oxygen peroxide. Since $K_2Ta_2O_6$ has a pyroclore like structure and one oxygen

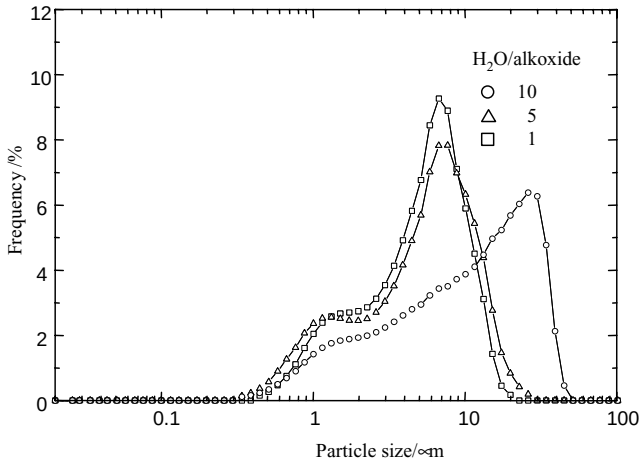

Fig. 9. Particle size distribution at H_2O/alkoxide ration of 1, 5, and 10.

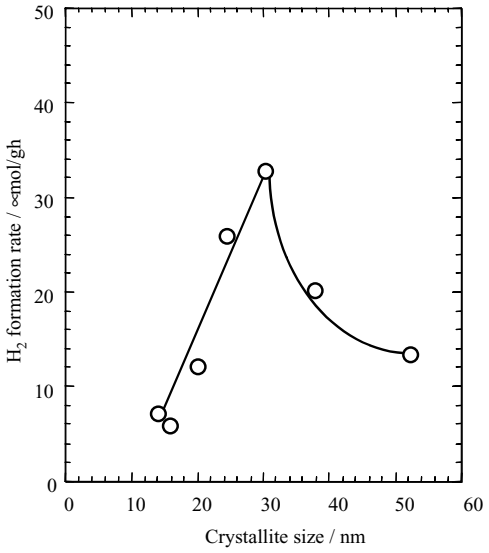

Fig. 10. Effects of crystallite size on H_2 formation rates on $K_2Ta_2O_6$ catalyst.

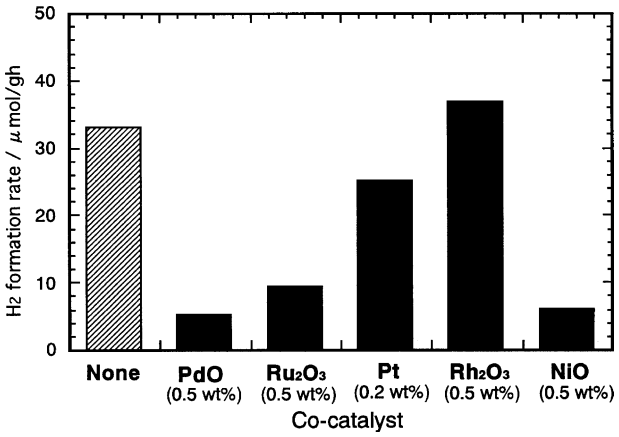

Fig. 11. Comparison of H_2 formation rate on metal-loaded $K_2Ta_2O_6$ to H_2O photolysis.

is originally missing, the formed oxygen my trap at the oxygen vacancy in $K_2Ta_2O_6$. Consequently, it is considered that the amount of oxygen formation might be smaller than that of H_2 formation and the catalytic activity may decrease after further longer period by the accumulation of oxygen. However, formation of H_2 and O_2 was observed over 24 h examined and the total molar amount of hydrogen becomes larger than that of the catalyst used. In addition, it was confirmed that no H_2 and O_2 was formed without irradiation of light. Therefore, it is seen that $Rh_2O_3/K_2Ta_2O_6$ can catalytically decompose H_2O into H_2 and O_2. In any case, it is seen that $Rh_2O_3/K_2Ta_2O_6$ exhibits the activity to the photocatalytic decomposition of H_2O into H_2 and O_2. Considering the absorption edge (230 nm), it is expected that the further higher H_2 formation rate in H_2O decomposition my be achieved by using UV light for a light source. This is now under investigation.

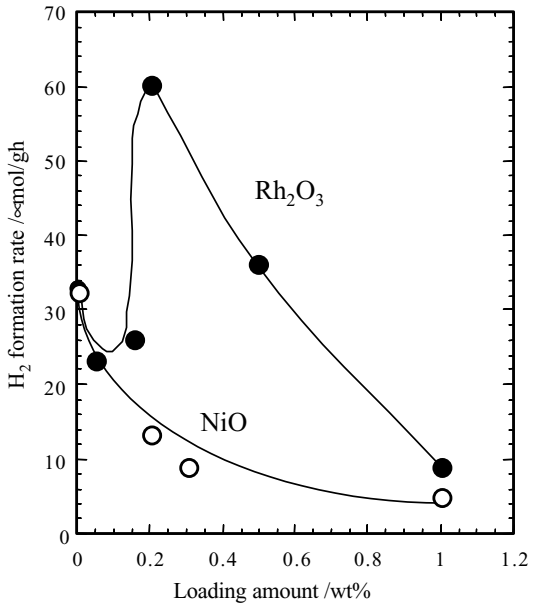

Fig. 12. H_2 formation rate as a function of Rh_2O_3 loading on $K_2Ta_2O_6$.

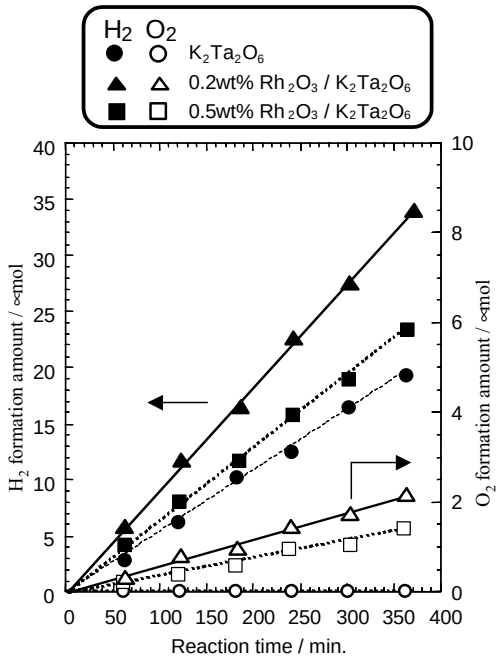

Fig. 13. H_2 and O_2 formation amount as a function of reaction time on $Rh_2O_3/K_2Ta_2O_6$.

4. Conclusion

K–Ta mixed oxides with different crystal structure, $KTaO_3$ and $K_2Ta_2O_6$, have been prepared by alkoxide method. It was found that single phases of $K_2Ta_2O_6$ and $KTaO_3$ were obtained by the hydrolysis of K–Ta mixed ethoxides. In particular, $K_2Ta_2O_6$ single phase, which could not be obtained by the conventional solid-state reaction method was successfully prepared. The obtained $K_2Ta_2O_6$ exhibits much higher photocatalytic activity for H_2O decomposition than that of $KTaO_3$ without metal loading. Furthermore, photocatalytic activity of $K_2Ta_2O_6$ was strongly dependent on crystallite size. On the other hand, in order to clarify the origin for the difference in photolysis activity, the crystal structure and the band structure of $K_2Ta_2O_6$ were analyzed. As a result, its higher photocatalytic activity would be assigned to its higher energy for conduction band and it was found that optimized particle size exists. This study reveals that crystal structure as well as the particle size is important factor for increasing the photocatalytic activity to H_2O decomposition.

References

[1] S. Moon, H. Mametsuka, E. Suzuki, M. Anpo, Chem. Lett. (1998) 117–118.
[2] T. Takata, A. Tanaka, M. Hara, J.N. Kondo, K. Domen, Catal. Today 44 (1998) 17–26.
[3] K. Sayama, H. Arakawa, K. Domen, Catal. Today 28 (1996) 175–182.
[4] H. Kato, A. Kudo, Chem. Phys. Lett. 295 (1998) 487–492.
[5] H. Kato, A. Kudo, Catal. Lett. 58 (1999) 153–154.

[6] Z. Zou, J. Ye, K. Sayama, H. Arakawa, Nature 414 (2001) 625–627.
[7] T. Ishihara, H. Nishiguchi, K. Fukamachi, Y. Takita, J. Phys. Chem. 103 (1999) 1–3.
[8] C. Mitsui, H. Nishiguchi, K. Fukamachi, T. Ishihara, Y. Takita, Chem. Lett. (1999) 1327–1328.
[9] Z. Zhang, C.C. Wang, R. Zakaria, J.Y. Ying, J. Phys. Chem. B 102 (1998) 10871–10878.
[10] K.Y. Jung, S.B. Park, S.K. Ihm, Appl. Catal. A 224 (2002) 229–237.
[11] K. Hashimoto, A. Fujishima, Bull. Ceram. Soc. Jpn. 31 (1996) 815–820.
[12] Z. Ding, Q. Lu, P.F. Greenfield, J. Phys. Chem. B 104 (2000) 4815–4820.
[13] F. Izumi, J. Crystallogr. Assoc. Jpn 27 (1985) 23.
[14] A. Qteish, Rhys. Rev. B. 52 (1995) 14497–14504.
[15] M.A.Maki-Jaskari, T.T. Rantala, Phys. Rev. B. 64 (2001) 075407 (7 pages).
[16] A. Reisman, F. Holtzberg, M. Berkenblit, M. Berry, J. Am. Chem . Soc. 78 (1965) 4514–4520.
[17] International Tables for Crystallography, vol. A, The International Union of Crystallography, Kluwer Academic Publisher, 1996.
[18] Inorganic Crystal Structure Database, No. 2309.
[19] CPDS card No. 35-1464, X-ray Powder Data File, American Society for Testing and Materials, 1960.
[20] A. Kudo, H. Kato, S. Nakagawa, J. Phys. Chem. B 104 (2000) 571–575.
[21] Y. Inoue, Y. Asai, K, Sato, J. Chem. Soc. Faraday Trans. 90 (1994) 797–802.
[22] M. Khono, S. Ogura, K. Sato, Y. Inoue, Chem. Phys. Lett. 267 (1997) 72–76.
[23] H. Kato, A. Kudo, J. Phys. Chem. B 105 (2001) 4285–4292.
[24] A. Kudo, K. Sayama, A. Tanaka, K. Asakura, K. Domen, K. Maruya, T. Onishi, J. Catal. 120 (1989) 337–352.